

Article

Damage Monitoring of a Catenary Moored Spar Platform for Renewable Energy Devices

Deirdre O'Donnell ^{1,2,3}, Jimmy Murphy ⁴  and Vikram Pakrashi ^{1,2,3,*} 

¹ Dynamical Systems and Risk Laboratory, School of Mechanical and Materials Engineering, University College Dublin, Dublin 4, Ireland; deirdre.odonnell@ucdconnect.ie

² Marine and Science Foundation Ireland Centre Marine & Renewable Energy Ireland (MaREI), University College Dublin, Dublin 4, Ireland

³ The Energy Institute, University College Dublin, Dublin 4, Ireland

⁴ MaREI Centre, Beaufort Building, University College Cork, Haubowline Road, Ringaskiddy, Co., Cork P43 C573, Ireland; Jimmy.murphy@ucc.ie

* Correspondence: Vikram.Pakrashi@ucd.ie; Tel.: +353-1-716-1833

Received: 29 May 2020; Accepted: 9 July 2020; Published: 14 July 2020



Abstract: Structural performance of renewable energy device platforms is central to their power generation in a reliable and competitive manner. However, there is a gap in research in the conceptual and experimental stages of such devices at lower technological readiness levels in terms of understanding of their structural responses. Uncertainties around knowledge related to damage conditions of such structures are under-researched and experimental investigations into the monitoring of performance of such structures are significantly needed. This research addresses this need and investigates various damage conditions in a scaled catenary moored spar platform in an ocean wave basin, exposed to typical wave conditions for the west coast of Ireland. A comparison of the monitored structural responses was carried out with respect to the undamaged experimental model. It was observed that while free decay tests were not useful to distinguish between various damage levels, a characterisation of the distribution of the responses can be relevant in identifying damages or significant structural changes. The work contributes to the much-needed experimental evidence base around structural health monitoring of renewable energy device platforms.

Keywords: spar platform; mooring; damage; structural health monitoring; uncertainty; renewable energy; ocean wave basin

1. Introduction

Safe and efficient performance of offshore renewable energy devices can be linked to the exposure scenarios they face over lifetime [1–3]. It is thus important to understand the structural responses of such devices [4–6] due to these exposure scenarios. While this importance is well acknowledged, there is no straightforward way to achieve it. Variabilities and uncertainties of the exposure conditions over their lifetime [7], along with the evolution of technological readiness present several challenges [8]. While natural exposure conditions and their variabilities cannot be changed, the understanding of the structural responses during the evolution of technological readiness can be improved significantly.

Renewable energy devices typically go through a number of technological readiness levels at smaller scales before they are tested in the ocean at full scale. Several interpretations and decisions regarding their structural responses are thus taken through the analyses of scaled testing in ocean wave basins and flumes. While some guidelines around such scaling exist [9], it is not straightforward to scale up ocean wave basin responses to full scale structures, nor is it easy to model every aspect of the structure numerically. In addition, there remain the challenge of stochasticity present in ocean waves [10].

A particular challenge in relation to the lifetime responses of these offshore renewable energy device platforms is the understanding of damage. The term platform used in this paper refers to the physical structure to which a device is connected. Offshore renewable energy is a rapidly burgeoning field, and while a wide range of designs are available, the focus has been primarily on producing as high energy as possible per unit structural [11]. This has led the platforms to be extremely flexible and they often behave nonlinearly during their normal operational phase [12]. While damage analysis is acknowledged as an important part of design of such structures for actual deployment, their nature and consequences are still defined in a limited way. Existing numerical studies have tried to address some of these issues [13–17], but there is a significant paucity of literature in relation to existing experimental evidence based around this topic.

A scaled tripod [18] analysis on fatigue damage focuses on statistical techniques of detection. Experiments on damaged ship beam [19], loading for tidal turbines [20] and monitoring of responses of renewable energy platforms or its control [21–23] are present, but there is no damage-specific variability study to the best of the knowledge of the authors. Experimental studies of damage responses and the variability of such responses of offshore renewable energy platforms can lead to guidelines and recommendations for scaled testing, and lifetime risks can be better understood at lower technological readiness levels. It would also address some of the epistemic uncertainty that exists around the responses to damages over operational lifetime [24–27]. Such experiments would also eventually be used to calibrate numerical simulations against extreme value responses [28]. Scaled experiments on damage can provide better monitoring markers [29,30] and allow taking informed decisions on the technological progress of devices, thereby avoiding investment in structurally less favourable designs, irrespective of their potential for harnessing energy. Such testing can also be helpful when new materials [31], designs [32] or operations [33] are proposed.

This paper addresses a gap in the literature regarding experimental evidence based on damage responses for offshore renewable energy device platforms by carrying out targeted tests and analyses on a spar-type platform in an ocean wave basin for a range of damage scenarios. The term damage is considered from a wide sense of interpretation and is linked to aspects that potentially affect the structure from a mechanical point of view in terms of stability and potential collapse, with significant consequences around safety and operations. Fixed monopiles [11] can be particularly susceptible to scour and the change in natural frequencies can be relevant [34]. However, there are challenges in terms of the variability of these natural frequencies as damage markers due to environmental and tidal effects [35]. Experimental validation of such monopiles will thus depend, amongst other aspects, on the fundamental understanding of how soil models and the interaction between soil and structure can be scaled up. For floating turbines, on the other hand, instability and collapse are of significant relevance. The loss of one of the tension legs or mooring lines [32,33] are already established in developing a technology to be an important aspect to consider and has been numerically investigated for various damage levels [36]. In this regard, especially for spar-type solutions, the effect of instability from unwanted and uneven distribution of moment of inertia is another problem. A comparison between a spar-buoy and a semi-submersible platform [37] indicates that the spar-buoy's responses will be significantly affected by such changes. An experimental investigation into such variations in inertia and related tilt can be brought about by adding small masses to the experimental platforms and also by varying the uniformity of ballasting. Mass and inertia imbalance may be due to localised damage and consequent flooding, potentially compromising safety [38]. Localised flooding and related stability analyses have been considered before in design [39]. While a semi-submersible solution would be more susceptible to such cases, for a range of smaller-scale models, the addition of mass can provide first indications around some of the flooding effects. Essentially, irrespective of a design example, flooding due to technical or operational problems with the ballast system or otherwise can lead to such unwanted structural responses [40]. It is then important to consider such changes to relevant load combinations, as still water loading can also contribute to impact on the overall safety [41]. Thus,

the consideration of such damage conditions and their representations are linked to accidental and damage-loading conditions.

The experimental results in this paper address this imbalance of mass and moment of inertia, along with the loss of mooring lines. The work not only creates an initial benchmark around such damage investigations but also generates the possibility of carrying out extensive studies around scaled testing for estimating lifetime performance for renewable energy device platforms in the future. Such investigations have the potential to reduce both capital expenditure at a design stage and operational expenditure during the service life, thereby leading to more competitive levelized costs of energy [42]. Studies like the one presented in this paper are thus fundamental in experimentally understanding uncertainties and its reduction for the renewable energy sector.

The significance of this work can be interpreted from three aspects: First, despite the rapid evolution of offshore wind turbines and other renewable energy devices, the decisions around the development of such technology will have to be made through scaled tests in wave basins and flumes. This work emphasises and contributes to the needs of assimilating the damage scenarios and its detection, along with the challenges and limitations of such detection in these scaled tests. It is expected that future work along this direction will eventually create a benchmark not only for damage detection, but for creating a protocol for reproducing damage at a scaled level. Secondly, this work investigates various approaches and markers for the detection of damage by investigating the dynamic response signatures in both time and frequency domains at a fundamental level. While a vast literature exists overall in the field of damage detection of various structures, eventually their purpose is in amplifying fundamental differences observed in time and frequency domains between damaged and undamaged scenarios to create a consistent and robust marker. To this effect, this paper provides a first estimate of the types of changes that can be expected due to certain damages and where their limitations are. These observations will guide future investigations into the development of both algorithms and markers of damage detection. Finally, the lifetime structural performance of structures is fundamentally related to the extremes of the distributions of their dynamic responses and the changes to such extremes can be related to the structural reliability index. This work demonstrates, from scaled testing and limited measurements, how such changes of the response histograms take place due to damages in the fitted extremes. This observation will be particularly relevant in developing reliability and fragility measures of the structure in the future and similar studies can also act as an input to fatigue analysis models.

2. Experimental Details

To address and understand the variability and uncertainty related to damage conditions in a floating platform, a range of scaled experiments were carried out on a scaled model of a floating spar platform in an ocean wave basin under a chosen set of ocean wave test conditions. These experiments are typical for progress through various technological readiness levels (TRLs).

2.1. Deep Ocean Wave Basin

Tank testing was carried out in the deep ocean wave basin at the Lir National Ocean Test Facility, Ireland. The tank is 12 m wide and 30 m in length. It has a movable floor with depths up to 3 m and is fitted with 16 hinge force feedback paddles capable of producing scaled, regular and irregular waves up to 1.1 m in height.

Two 22.5 N Load cells (Futek LSB210, Irvine, CA 92618, USA) were attached to the port and starboard lines, respectively, and one 44.5 N cell was attached to the stern line to measure the changes in mooring force. A system of four cameras was mounted on a truss system above the tank, and tracked platform motion on four reflective markers attached to the platform in two different vertical planes using a calibrated system. Resistive wave probes (1 m long) controlled by a control wave monitor unit recorded the surface elevation of the water along the tank, one of which was in line with the position

of the floating spar. The wave probes were calibrated by comparing voltage readings against known changes in water elevation [43,44].

2.2. Floating Spar Buoy Platform Model

The Froude-scaled [45] floating spar platform (1:36 of full scale) had a mass of 55 kg and consisted of a cylindrical casing of approximately 250 mm diameter and 1.531 m in height, with a series of internal weights and ballasts (Figure 1). The choice of this floating spar platform is guided by the fact that it is a particularly viable and popular form of design of offshore wind [46,47] and due to the feasibility of developing a scaled model for this platform for testing in the wave basin. The inclusion of other designs in a similar testing format in the future will significantly augment the understanding and quantifiable impacts of various forms of damage on their performance over the lifetime.

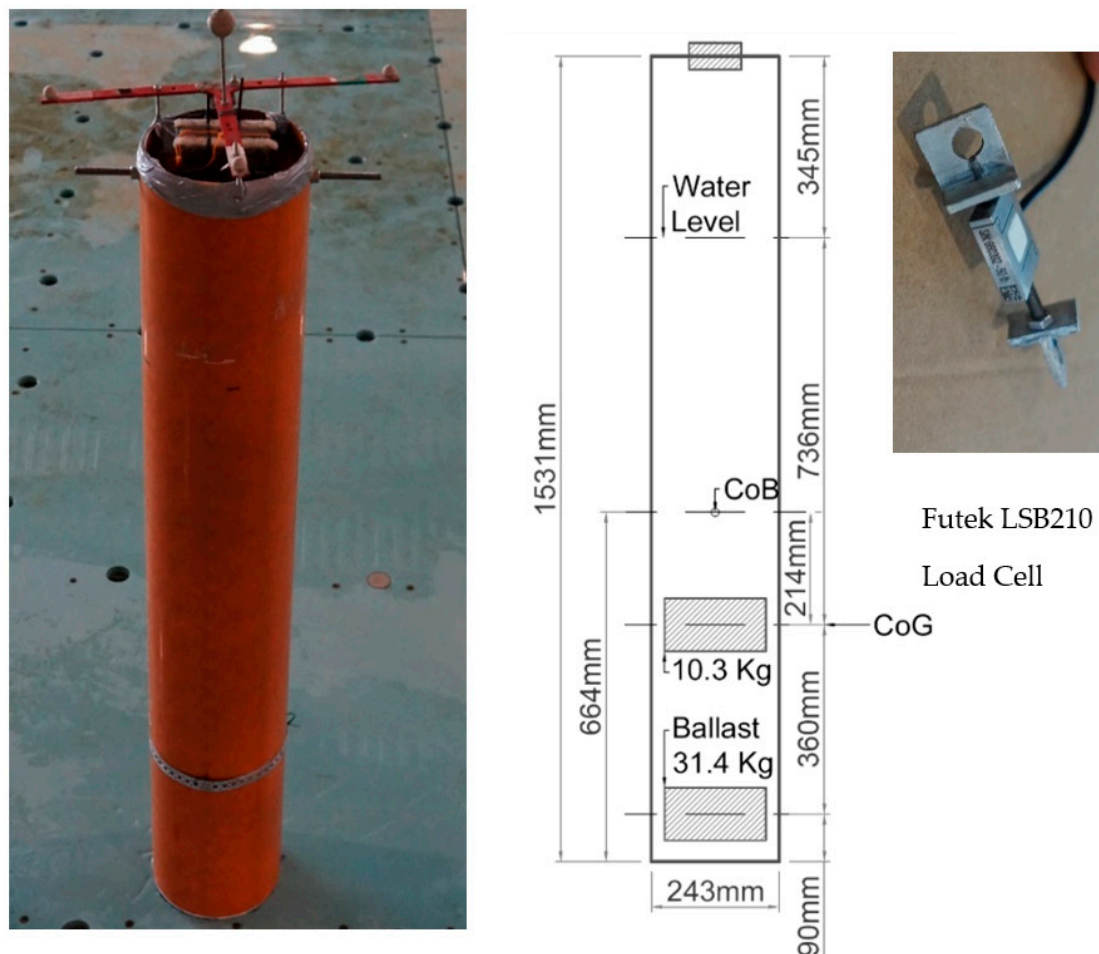


Figure 1. Spar buoy platform model photograph and drawing.

2.3. Mooring System Design

The mooring system consisted of three catenary mooring lines. The front two lines were spring-taut, with a spring constant 6.93 N/m approximating the linear best fit load-displacement curve of the numerically designed catenary line (Figure 2). The custom-made spring for the experiment had a constant stiffness of 5.1 N/m.

To prevent the spring from overextending, a string was tied to both ends of the spring at a length specified by the manufacturer as being within the extension limits. To form the rest of the mooring line, a mooring chain threaded with steel wire was used, designed to be a geometrically representative Froude-scaled weight. For a full scale 60 mm diameter mooring chain line of 71.64 kg/m,

the model-scaled mass per unit length was 55 g/m. Table 1 presents the values in the scaled physical model for testing.

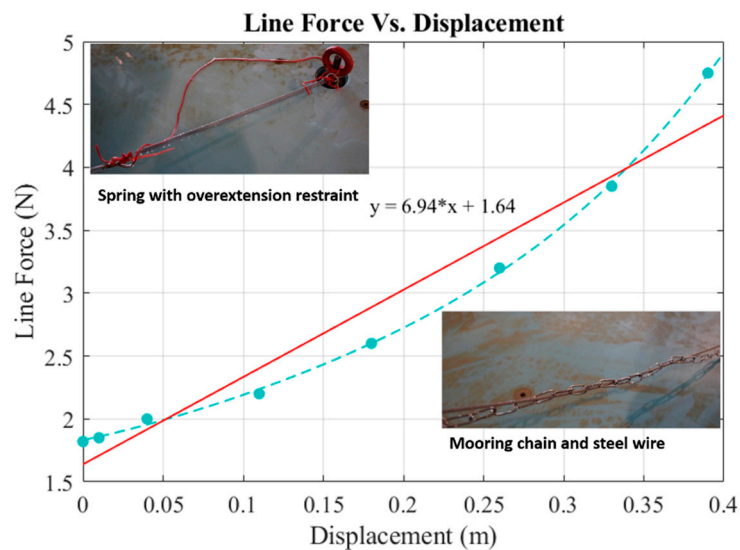


Figure 2. Best-fit approximation of the spring constant of the designed mooring lines.

Table 1. Scaled Mooring Line Mass.

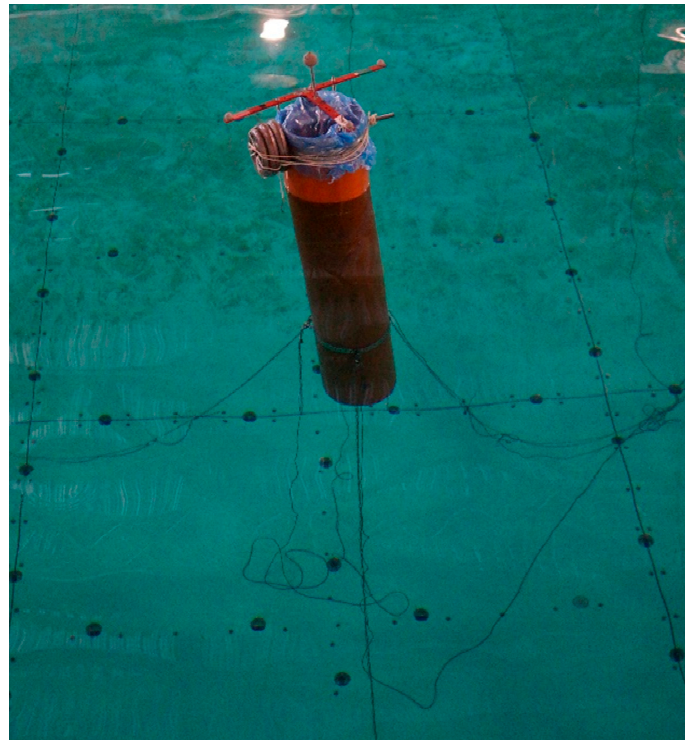
Location	Line Length (m)	Measured Line Mass (g)	Mass per Metre (g/m)
Port	4.4	250	56.8
Starboard	4.4	251	57.0
Stern/Catenary Line	14.6	880	60.3
Average			58.03

2.4. Structural Configurations Representing Damage Effects

The structure was tested in various phases (Phases A–F) to represent different levels and forms of damage, as presented in Table 2, in the form of structural modifications. The undamaged state (Phase A) provides a baseline from which the effect of all subsequent structural modifications can be assessed. Damaged Phases B, C and D change the platform weight and subsequently, the draft. Such conditions could be experienced if the chambers of the platform were to become partially filled with water due to some damage to the structure, or unexpected failure of a mooring line causing asymmetrical restraining forces and subsequent banking of the platform. In Phase B, a 2.5 kg weight is added to the upper port side of the platform, causing a larger draft and the platform to bank to the left when in still water. Phase C involves adding an extra weight of 1.25 kg to the upper port side of the platform, causing a further increase in the draft and greater tilt of the floating platform. Phase D weighed the platform with an extra 2.5 kg on the upper part of each side of the platform, causing the largest draft of the three added-weight configurations while the platform remained vertical, in order to investigate the effect of draft increase without the instability from asymmetry. In Phases E and F, different mooring lines were severed to analyse the structure’s reaction to a failure, as the Det Norske Veritas (DNV) code ST-0119 (superseding OS-J103) outlines for accidental limit state design. The severed back mooring line is the least critical line, as it lies in line with the direction of the oncoming waves, and phase E aims to discover what effect (if any) the removal of this line will have on the overall response of the platform. The front two mooring lines are responsible for a higher share resistance against oncoming waves, and Phase F simulates what would happen if one of these were to fail. As an example, the testing of the platform in Phase C is presented in Figure 3.

Table 2. Structural configurations for different test phases representing damage.

Phase	Description
A	Original configuration
B	Asymmetrically over-weighted +2.5 kg
C	Asymmetrically over-weighted +3.75 kg
D	Symmetrically over-weighted +5 kg
E	Severed back mooring line
F	Severed front mooring line

**Figure 3.** Platform configuration during Phase C testing.

2.5. Wave Conditions

The spar was tested under a selection of both regular and irregular wave conditions to represent a range of real sea conditions, typically found at the Atlantic Marine Energy Test Site (AMETS) off the coast of Belmullet, Co. Mayo, Ireland. Sinusoidal waves were also used to obtain the dynamic responses of the platform, and the parameters for such waves were selected to represent the range of wave periods and heights expected at full scale. The Bretschneider spectrum (also known as the modified Pierson–Moskowitz spectrum) was used for testing, as it most closely models the irregular wave behaviour in this area with its spectrum $S(f)$ represented as

$$S(f) = \frac{5}{16} H_S^2 f_P^4 f^{-5} \exp\left(\frac{-5}{4} \left[\frac{f}{f_P}\right]^{-4}\right) \quad (1)$$

where f is the frequency, f_P is the peak frequency and H_S is the significant wave height [48]. A scatterplot, obtained from data at Berth B in Belmullet between 1 September 2012 and 16 October 2014, was used to determine a representative set of waves. Figure 4 shows significant wave height (H_S) against mean period (T_Z), and the percentage of occurrence of each wave case defined by these two parameters.

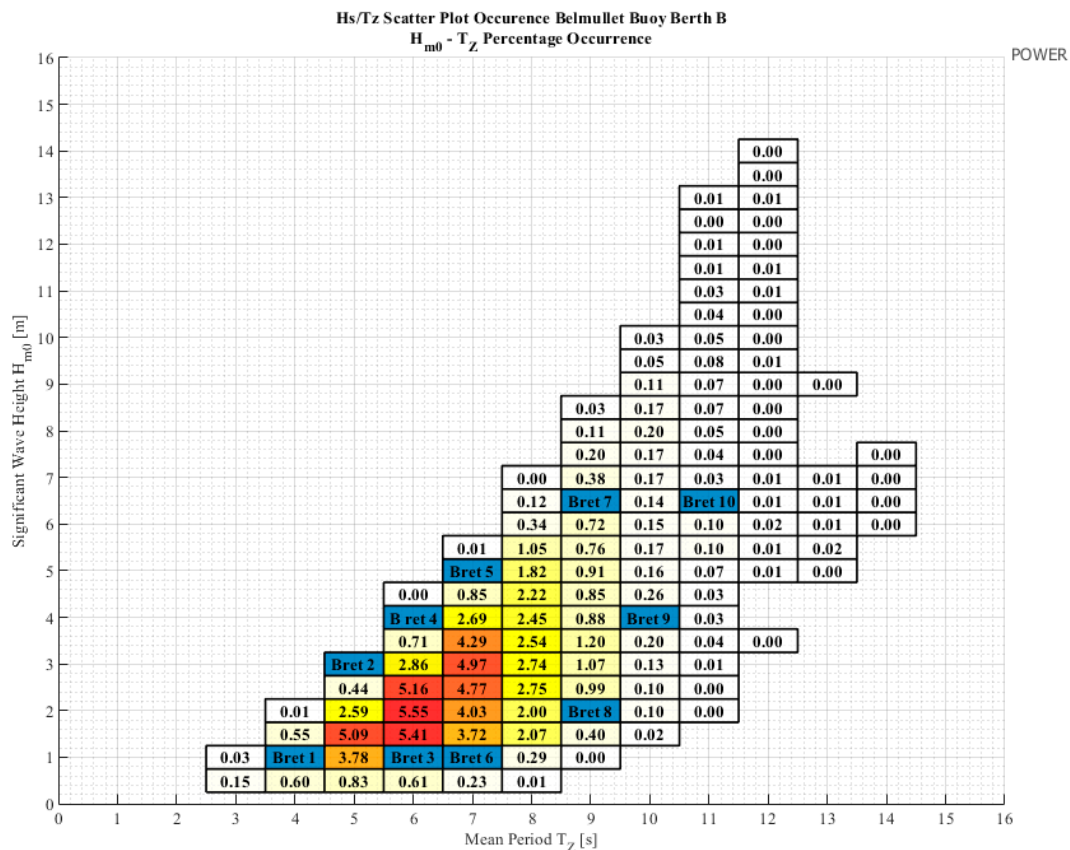


Figure 4. Scatterplot of waves at Belmullet showing the range of selected test cases.

A conversion factor [49] linked the peak period (T_P), defining the spectrum in the wave basin, to the energy period (T_E) as

$$T_P = 1.175T_E \tag{2}$$

For Bretschneider spectrum,

$$T_E = 1.206T_{02} \tag{3}$$

where T_{02} is the spectral equivalent to T_Z .

This leads to

$$T_P = 1.42T_{02} = 1.42T_Z \tag{4}$$

The mean period, T_Z , identified from the scatterplot, and the relationship between it and the peak period, $T_P = 1.42 T_Z$, are then used to decide the peak of the periods used in testing. The wave conditions chosen (Table 3) for the tests cover range of the most common wave conditions.

Each irregular Bretschneider wave test was run for 326 s. The first 10 s were still water recording, followed by the start of the wave paddles which were allowed to run for one minute for the waves to be established (i.e., reflected waves and input waves all acting on the system). Subsequently, 256 s of data were recorded for the test, which is the minimum repeat time for the entire time series generated. At the end, a 60 s period of settling time was allowed for recording after the wave maker stopped. Figure 5 presents a comparison between the output of the wave paddles with intended surface elevation values and the surface elevation recorded by the wave probes. The small errors are attributed to wave reflection within the tank. Figure 6 presents the same comparison in the frequency domain and an agreement between the two is observed. Incident and reflected waves are not distinguished by a reflection analysis when analysing platform motion. While in some cases it is preferable to know the incident wave height and to use this for analysis (e.g., for long vessels), since it has a bearing on

hydrodynamic analyses, the floating spar platform is relatively small compared to the wavelength for tests and is governed by the buoyancy force, which is related to the surface elevation at that point.

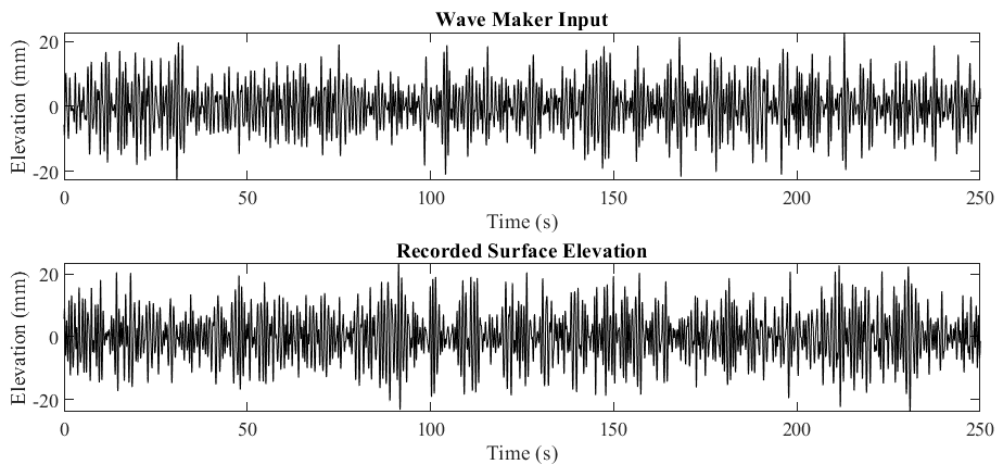


Figure 5. Designed and recorded wave surface elevation for the Bretschneider spectra.

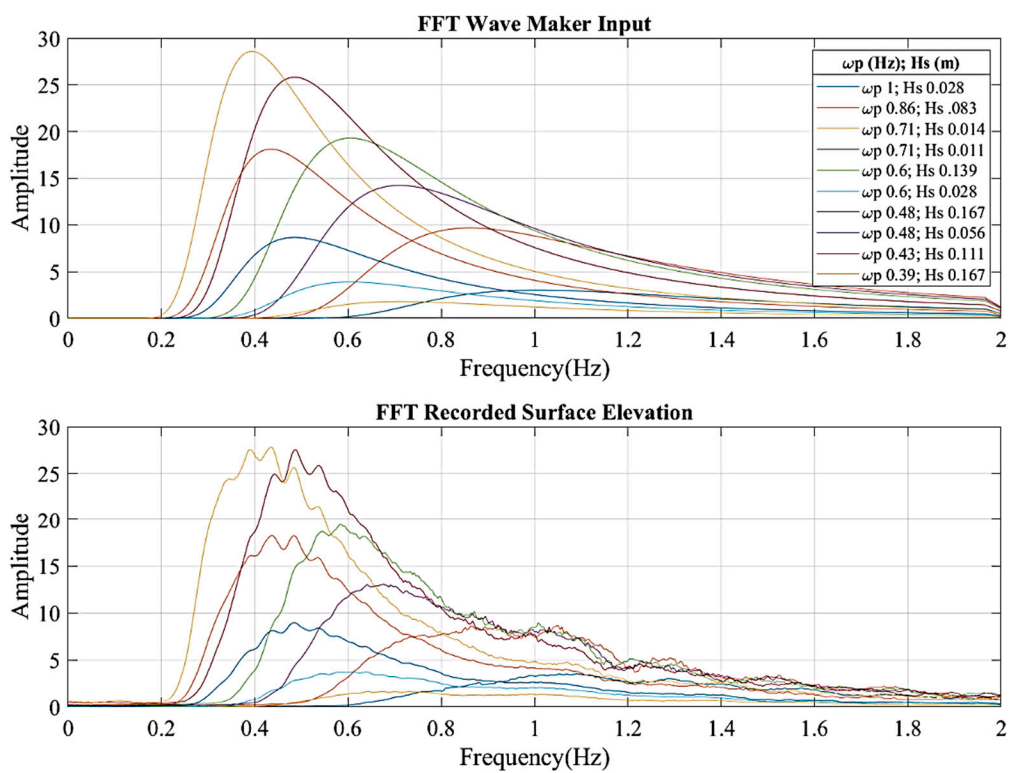


Figure 6. Frequency comparison of wave basin surface elevation of test waves between designed and recorded data.

Table 3. Selected wave cases at ocean basin testing model scale.

Wave Case	Full Scale			Model Scale		
	T_p (s)	f_p (Hz)	H_s (m)	T_p (s)	ω_p (Hz)	H_s (m)
Sine 1	4	0.25	0.5	0.667	1.50	0.014
Sine 2	5	0.2	1	0.833	1.20	0.028
Sine 3	6	0.167	1	1.000	1.00	0.028
Sine 4	7	0.143	1.5	1.167	0.86	0.0415
Sine 5	8	0.125	2	1.333	0.75	0.0555
Sine 6	10	0.1	2	1.667	0.60	0.0555
	T_p (s)	f_p (Hz)	H_{m0} (m)	T_p (s)	ω_p (Hz)	H_{m0} (m)
Bret 1	6	0.167	1	1.000	1.00	0.028
Bret 2	7	0.143	3	1.167	0.86	0.083
Bret 3	8.5	0.118	0.5	1.417	0.71	0.014
Bret 4	8.5	0.118	4	1.417	0.71	0.111
Bret 5	10	0.1	5	1.667	0.60	0.139
Bret 6	10	0.1	1	1.667	0.60	0.028
Bret 7	12.5	0.08	6	2.083	0.48	0.167
Bret 8	12.5	0.08	2	2.083	0.48	0.056
Bret 9	14.0	0.071	4	2.333	0.43	0.111
Bret 10	15.5	0.065	6	2.583	0.39	0.167

Each regular wave was run for 200 s with 10 s of still water recording at the beginning, 130 s of testing and 60 s of settling down time at the end after the wave paddles stopped.

2.6. Data Acquisition

An optical system (Qualisys Tracker Manager, Qualisys AB, Kvarnbergsgatan 2, 411 05 Göteborg, Sweden) interface collated 3D positional data from the camera system in the wave basin, ensuring that the reflective markers on the structure were always within range of the cameras. The centre of gravity was recalculated for each phase of testing during data acquisition. Acceleration response was derived for each monitored point and responses for the upper mid-point of the spar platform was considered for analysis in this paper. Measurements from wave probes 1–6, and load cells 1–3 were recorded with Labview. Each sensor was calibrated before testing and checks such as still water measurements were carried out during testing to ensure that measurements remained consistent and accurate throughout. Occasional unrealistic peaks were averaged and detrended to obtain displacements of about a zero mean.

3. Response Characterisation of the Test Platform

The test platform responses were characterised using free decay tests and wave tests in its various damage phases.

3.1. Estimation of Natural Frequency from Free Decay Tests

Free decay testing for displacement (sway, surge, heave) and rotation (pitch, roll, yaw) was conducted in still water to characterise the response of the test platform for each structural modification related to the damage phases. Fast Fourier transform (FFT) was used to pick the dominant frequency as the natural frequency of the platform. Due to rotational symmetry and main coupling effects, heave and pitch motions were mainly studied for spar platforms [50–52]. For a spar platform, where the geometry is the same for both surge and sway motions, it is reasonable to expect them to be representative of one another. The identified natural frequencies for the heave response are shown in Figure 7 and the range is observed to be between 0.4225 to 0.4444 Hz. It is observed that the various damage configurations did not relate to change in a significant change of natural frequencies. The estimated natural frequencies corresponding to heave, sway, surge and pitch are summarised in Table 4.

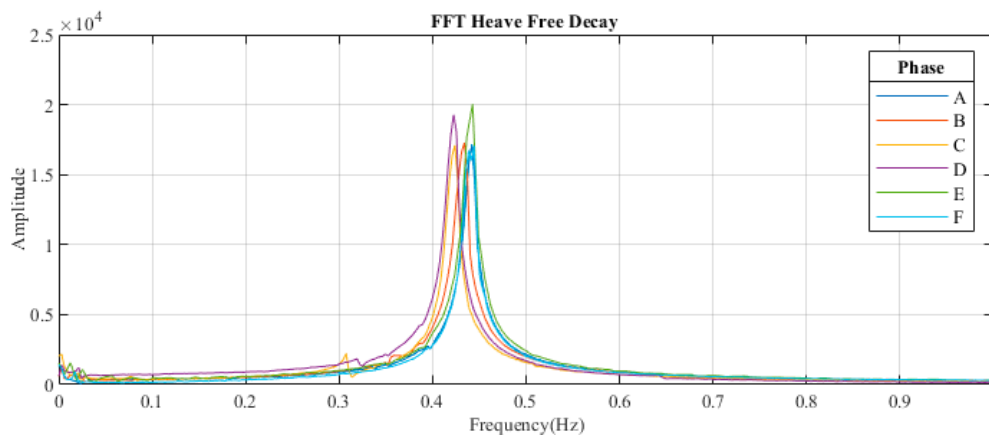


Figure 7. Fast Fourier transform (FFT) of free decay of heave motion for all phases of testing.

Table 4. Estimated natural frequency of heave, surge, sway and pitch motions.

Phase	Peak Frequencies from FFT (Hz)							
	Tank Scale				Full Scale			
	Heave	Sway	Surge	Pitch	Heave	Sway	Surge	Pitch
A	0.444	0.026	0.029	0.397	0.0740	0.0043	0.0048	0.0662
B	0.434	0.016	0.021	0.368	0.0723	0.0027	0.0035	0.0613
C	0.424	0.023	0.021	0.0596	0.0707	0.0038	0.0035	0.0099
D	0.423	0.021	0.021	0.316	0.0705	0.0035	0.0035	0.0527
E	0.443	0.021	0.012	0.391	0.0738	0.0035	0.0020	0.0652
F	0.442	0.018	0.01	0.368	0.0737	0.0030	0.0017	0.0613

Surge (Figure 8) and sway (Figure 9) both had low frequencies and irregular decay responses, which is partially explained by the tendency of the spar to rotate slightly as it settled. The sway direction measured is relative to a fixed axis in the tank and a non-fixed axis on the device itself. Consequently, sway and surge motions were not individually distinguishable in some data. Despite the variations and uncertainties from standard testing procedure, the variation of the estimated natural frequencies was not high considering all phases of testing.

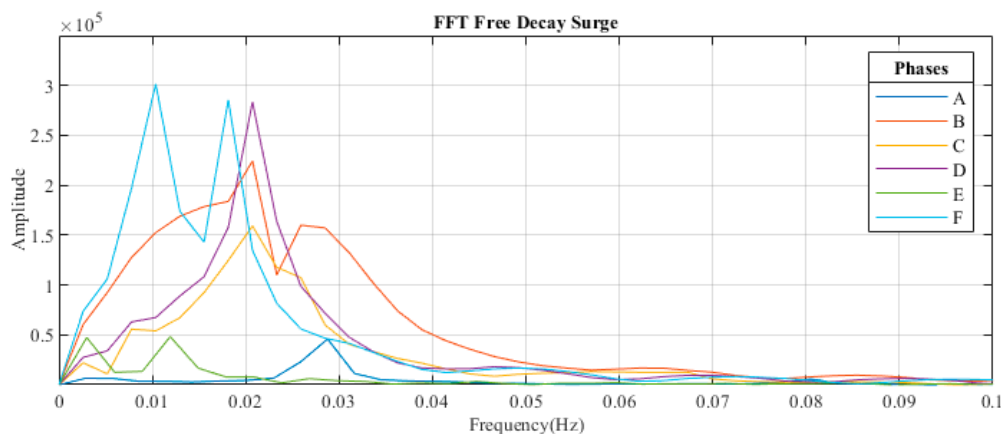


Figure 8. FFT of free decay of surge motion for all phases of testing.

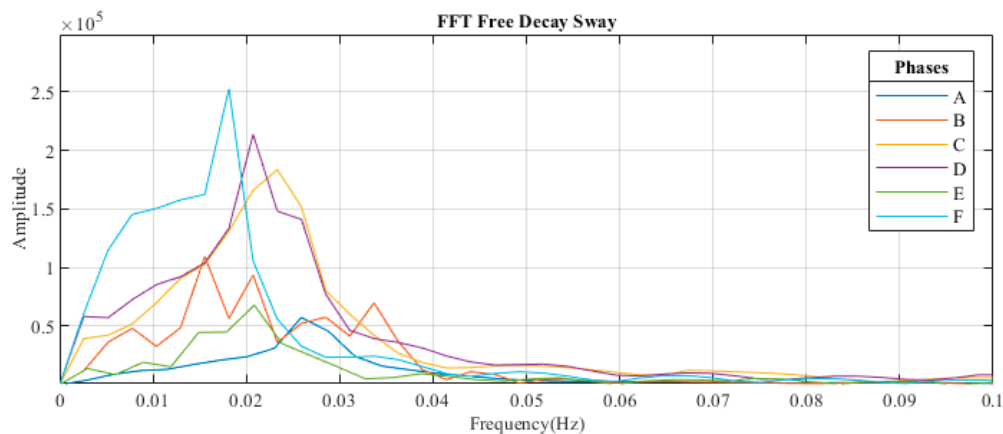


Figure 9. FFT of free decay of sway motion for all phases of testing.

The natural pitching frequency (Figure 10) for Phase C was considerably lower than all other phases, and this is due to a secondary forcing from an unsettled water surface. Otherwise, there was no notable reduction or increase in natural frequencies of any direction of motion among the various phases of testing.

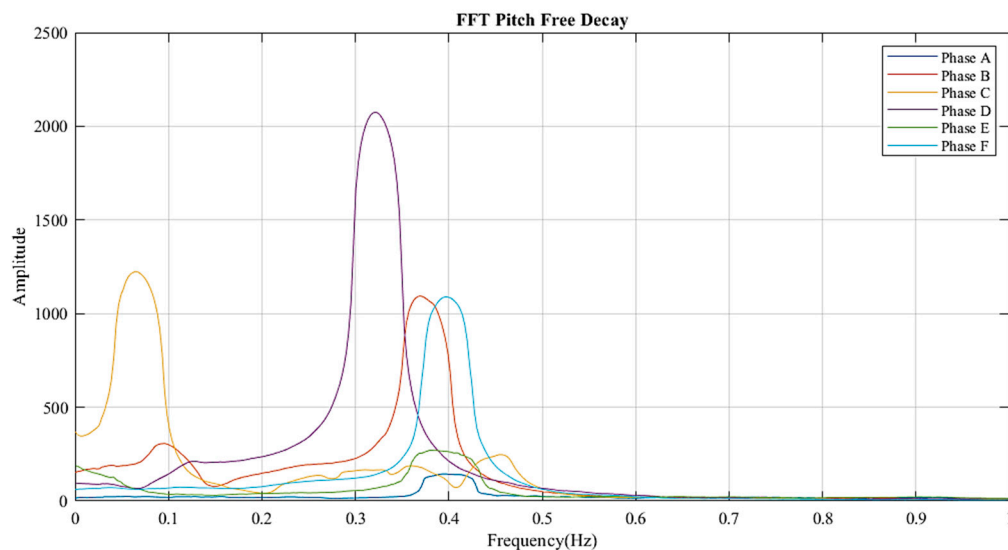


Figure 10. FFT of pitch of free decay for all phases of testing.

3.2. Estimation of Damping Ratio from Free Decay Tests

A basic logarithmic decrement approach was used to estimate equivalent viscous damping ratio of the platform for the various testing phases. Slamming of the waves causes friction damping and will be significantly higher. Consequently, these estimates only offer a potential comparison among the various damage phases. As an example, Figure 11 presents free decay responses for heave motion, while Table 5 presents the estimated averages of the equivalent viscous damping ratios.

The estimation of the equivalent viscous damping ratio for sway and surge motions is more variable due to the rotational tendency of the platform and thus is not consistent. Distribution of decay rate of damping for different damage states [53] has been investigated before as a novel way to identify damage using time domain data. However, with the low estimates of equivalent viscous damping ratio obtained (1.5% and less, excluding friction damping), it is observed to be unsuitable as a consistent marker of damage even when free decay tests are consistent.

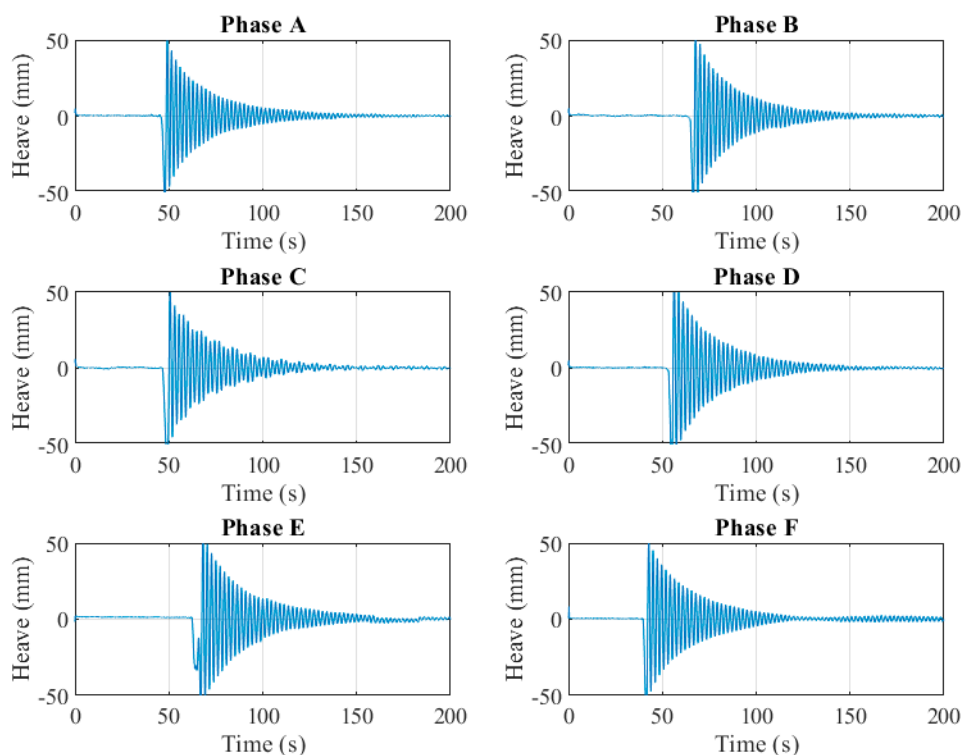


Figure 11. Heave response of platform to decay test for different phases.

Table 5. Heave damping ratio estimates.

Heave Response	Phase A	Phase B	Phase C	Phase D	Phase E
Average estimated ζ (%)	1.45%	1.50%	1.38%	1.60%	1.29%

4. Results

Statistical measures were computed as a marker to distinguish between various changes affecting the response of the platform. Such quality control type measures are popular in the structural health-monitoring literature, but they are also applicable in other domains and with different challenges of damages and other features of interest [54–56].

4.1. Quantiles of Acceleration Values

The time histories of the acceleration data recorded during wave tests were analysed to identify any significant changes among the various testing phases.

Figure 12 shows a sample time series for the floating platform for the same wave test (Bret 4) for different phases (A, B and C) of testing with various quantiles of the responses indicated on the figure. The changes are summarised for all wave tests and all phases in Figure 13. Relative changes to the mean and 95th percentile (p95) for each test were calculated with respect to the original undamaged state (Phase A). As seen in Figure 13, the vast majority of mean acceleration values change by +/-43%. Phases B, C, D, E and F change between +43% to +1%, +43% to +30%, +2% to -43%, -1% to +93% and -4% to -29%, respectively.

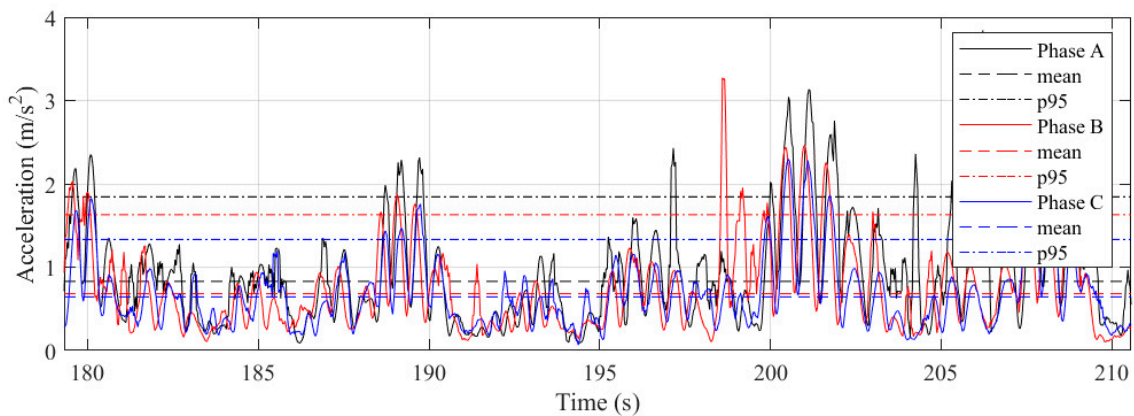


Figure 12. Comparison of acceleration time series with basic statistical measures for phases A, B and C excited by the Bret 4 wave.

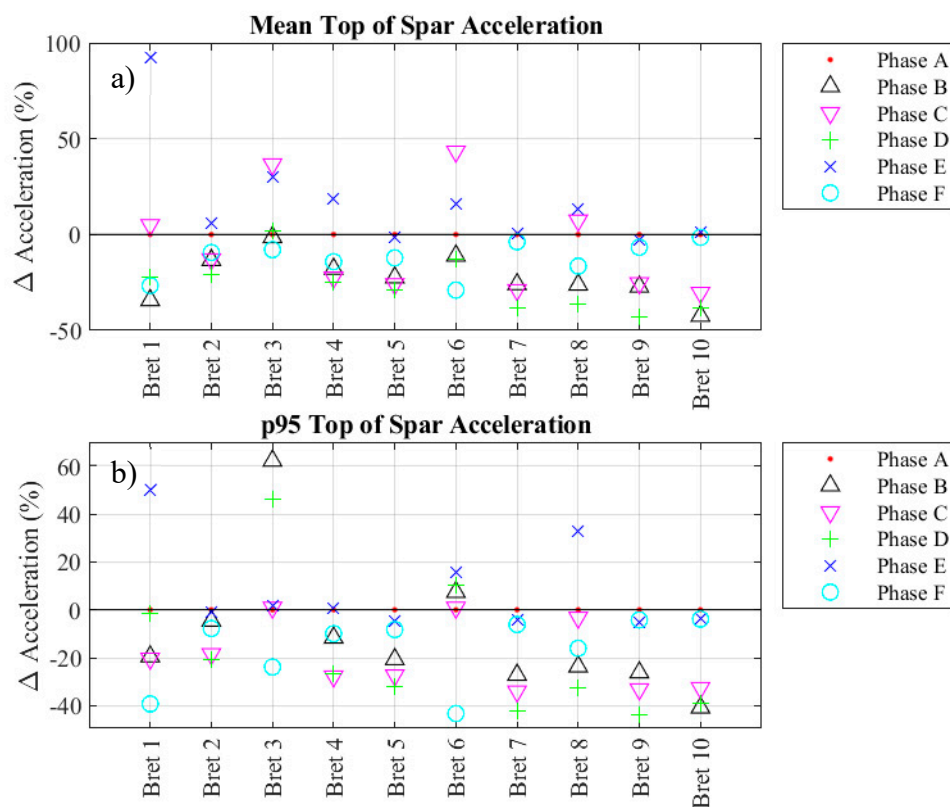


Figure 13. Relative changes in response acceleration between phases for Bretschneider wave excitation in terms of (a) mean values and (b) 95th percentile values.

Results for changes to the 95th percentile values for acceleration are also quite varied. Phases B, C, D, E and F see changes in p95 acceleration values between +62% to −27%, +1% to −34%, +46% to −44%, +50% to −4% and −4 to −43%, respectively. It is observed that while various changes of damages do change the quantiles of acceleration values significantly, calibration is required to make sense of them, and the excitation wave type is required to be known. It is difficult to distinguish between various damage causes only from the output response quantiles since different damage effects tend to overlap each other. Under such circumstances, it is only possible to assess an equivalent effect from a cause, rather than detecting it. The probabilities of crossing limits of such responses can still be computed since they can be specified without having to know the reason behind a certain damage or change

in platform structure and only deal with what response levels are not conducive to serviceability or safety of the structure. This is of significance since several other built infrastructure sectors [57,58] exhibit consistent changes in quantiles of responses in their operational conditions.

4.2. Probability Distribution Fits for Acceleration Responses

A probability distribution fit to observed data can often be a meaningful marker [59–61] for assessing various changes of damage conditions as compared to individual comparison of percentiles. Multiple distributions were considered for this data in this regard. A gamma distribution [62] was found an appropriate model for acceleration responses from an experimental model under irregular wave forcing. The probability density function (PDF) for gamma distribution for a random variable x is

$$f(x|a, b) = \frac{1}{b^a \Gamma(a)} x^{a-1} e^{-\frac{x}{b}} \quad (5)$$

where a is the scale parameter, b is the shape parameter and $\Gamma()$ is the gamma function. Weibull distributions are often a good fit to real engineering data [63] and valued for its adaptability. A Weibull has been shown to be a good fit for wave height data [64] but with issues related to predicting the extremes tails. The PDF of the Weibull distribution is

$$f(x|a, b) = \frac{b}{a} \left(\frac{x}{a}\right)^{b-1} e^{-(x/a)^b} \quad (6)$$

The general extreme value (GEV) distribution has been ubiquitous in modelling to include maximum values. Since these are what dictates limit states, this is of interest in a very wide range of engineering applications [28]. Since it is a generalisation of the Gumbel (encompassing the gamma distribution), Weibull and Frchet classes of distributions, it comes with more versatility in shape, but with potentially less definition. The PDF of the GEV is given by

$$f(x|k, \sigma, \mu) = \left(\frac{1}{\sigma}\right) \exp\left(-\left(1 + k \frac{(x - \mu)}{\sigma}\right)^{-\frac{1}{k}}\right) \left(1 + \frac{(x - \mu)}{\sigma}\right)^{-1 - \frac{1}{k}} \quad (7)$$

For

$$1 + k \frac{(x - \mu)}{\sigma} > 0 \quad (8)$$

where k is the shape parameter, σ is the scale parameter and μ is the location parameter.

The gamma, GEV, and Weibull distribution fits to the measured acceleration responses were compared in this paper, and Figure 14 provides an example of such a comparison.

The Bayesian information criterion (BIC) is chosen as the measure to assess the goodness of fit of a distribution. Using the optimised log likelihood value (L), and penalizing for the complexity of the model i.e., the number of parameters (N), and the number of observations (n), the formula for BIC is

$$\text{BIC} = 2(\log L) + (N * \log n) \quad (9)$$

The percentage difference in BIC between models is used as a measure to compare and rank the distribution fits with the lowest BIC value corresponding to the best fit, which is considered as a baseline. The other distributions are ranked in terms of BIC percentage differences from this best fit distribution with the lowest BIC. Table 6 presents the BIC differences for Phase A (undamaged) tests.

While a gamma distribution was most often found to be the best fit, an average across all tests indicate that a GEV distribution was most consistently able to represent the distribution of the data for all wave conditions. This was also observed to be true across all damage states and the GEV distribution for all phases are presented in Figure 15, as an example, for the Bret 8 wave.

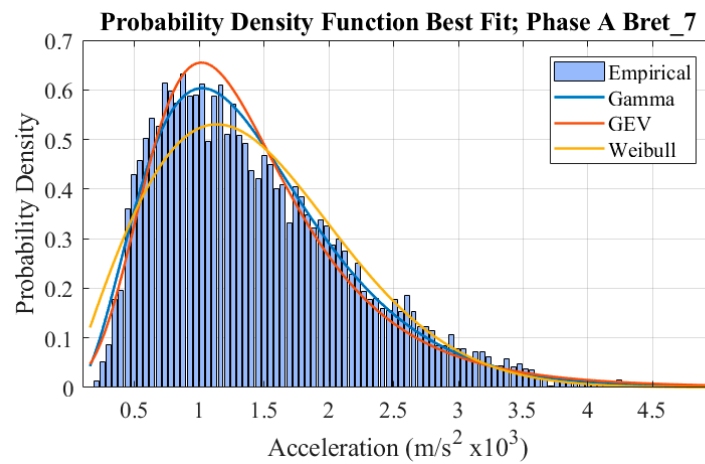


Figure 14. Comparison of gamma, general extreme value (GEV) and Weibull probability distributions fitted to acceleration responses for undamaged spar platform exposed to Bret 7 wave.

Table 6. Percentage difference of each Bayesian information criterion (BIC) value from best fit BIC value for different distributions for all Phase A tests.

Phase A	BIC Differences (%)		
	Gamma	GEV	Weibull
Bret 1	17.696	0	32.668
Bret 2	0	3.854	6.692
Bret 3	19.946	0	26.925
Bret 4	0	2.950	2.756
Bret 5	0	0.250	5.234
Bret 6	22.854	0	46.053
Bret 7	0	1.135	2.056
Bret 8	0	3.828	4.537
Bret 9	0	1.229	2.124
Bret 10	0	1.125	0.699
Average	6.050	1.437	12.974

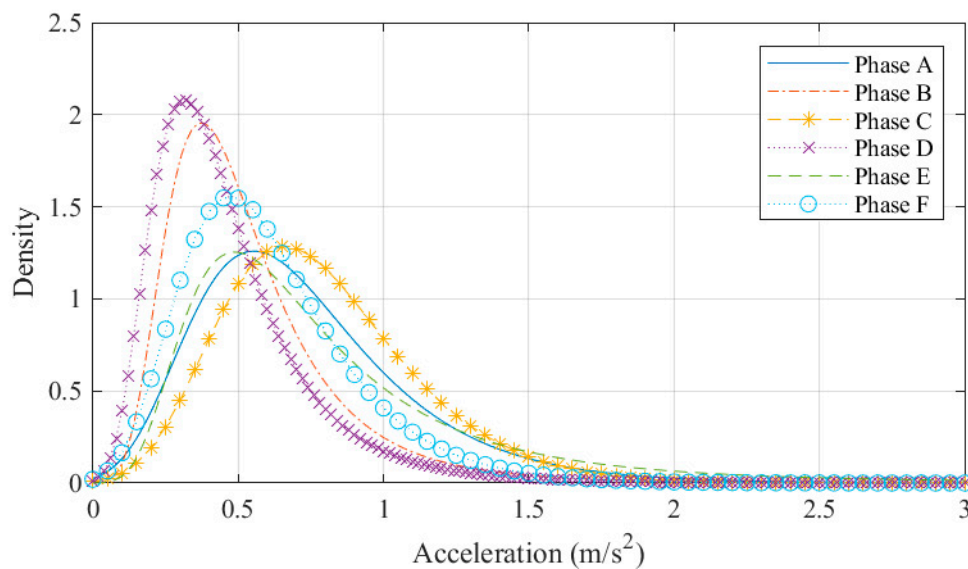


Figure 15. GEV fit for acceleration data for all phases of testing, for wave case Bret 8.

The changes to the data distribution across different damage states can be tracked visually to understand what changes lead to what type of changes in response. This can also be quantified through the changes of the distribution parameters of shape (k), scale (σ) and location (μ), defining each fit. A sample of these parameters and their changes between damage states is presented in Table 7. These parameters can be used to calculate comparative statistics (e.g., mean, variance), which can be used as further evidence of the goodness of fit of the models when compared to empirical values.

Table 7. Comparison of GEV distribution parameters for all phases for wave case Bret 7 and percentage change from Phase A.

<i>Bret 7</i>	Shape k	Scale σ	Location μ
Phase A	0.072	0.563	1.054
Phase B	0.051	0.414	0.792
	−29%	−26%	−25%
Phase C	0.042	0.361	0.787
	−42%	−36%	−25%
Phase D	−0.017	0.341	0.689
	−124%	−39%	−35%
Phase E	0.022	0.554	1.091
	−69%	−2%	+4%
Phase F	0.146	0.548	1.010
	+103%	−3%	−4%

Table 7 indicates significant changes in the three shape factors defining the distribution for each phase of testing. The shape factor (k), decreases up to −124% for phases B, C, D, E and increases by +103% for phase F. There are variations in the scale factor, which decreases by as much as −39%, and in the location factor where the variation is up to −39%. The shape factor is the most varied of the parameters and is the most descriptive in terms of changes to the distributions for different damage states.

The variation in the distribution parameters, when calibrated well, can thus be a better marker to distinguish between and even characterise the damage states.

4.3. Distribution of Extreme Values

Comparisons similar to the previous sub-sections were carried out on extreme value fits to the data, using a 95th percentile threshold (Figure 16). Extreme value fits have been observed to be reflective of changes in damage [28] for idealised mechanical systems. Comparing the difference between BIC values, the generalised Pareto distribution was observed to be the best fit, followed by the GEV. The generalised Pareto (GP) distribution uses all available data and not just block maxima like the GEV. It is characterised by a shape factor (k), also known as the tail index, and a scale parameter (σ). The threshold parameter (θ) is the value above which the distribution of the maxima is to be fit and defines the location of the distribution as

$$y = f(x|k, \sigma, \theta) = \left(\frac{1}{\sigma}\right) \left(1 + k \frac{(x - \theta)}{\sigma}\right)^{-1 - \frac{1}{k}} \quad (10)$$

Table 8 presents the GP distribution parameter values for various phases of testing, and the percentage difference of this value from Phase A. The shape factor (k) changes most significantly between phases. From an undamaged state, k decreases for all but phase F of testing, where it increases by 103.3%.

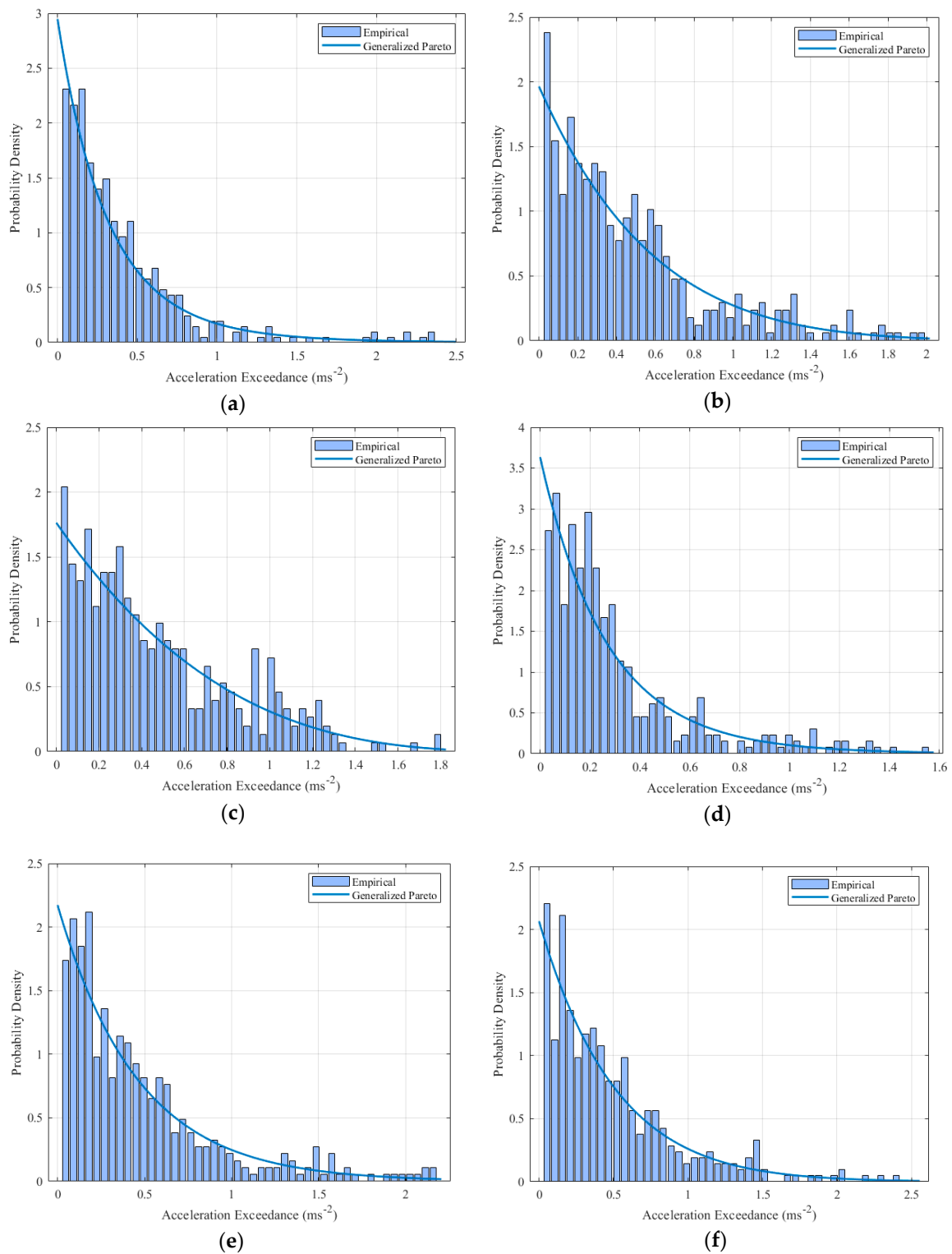
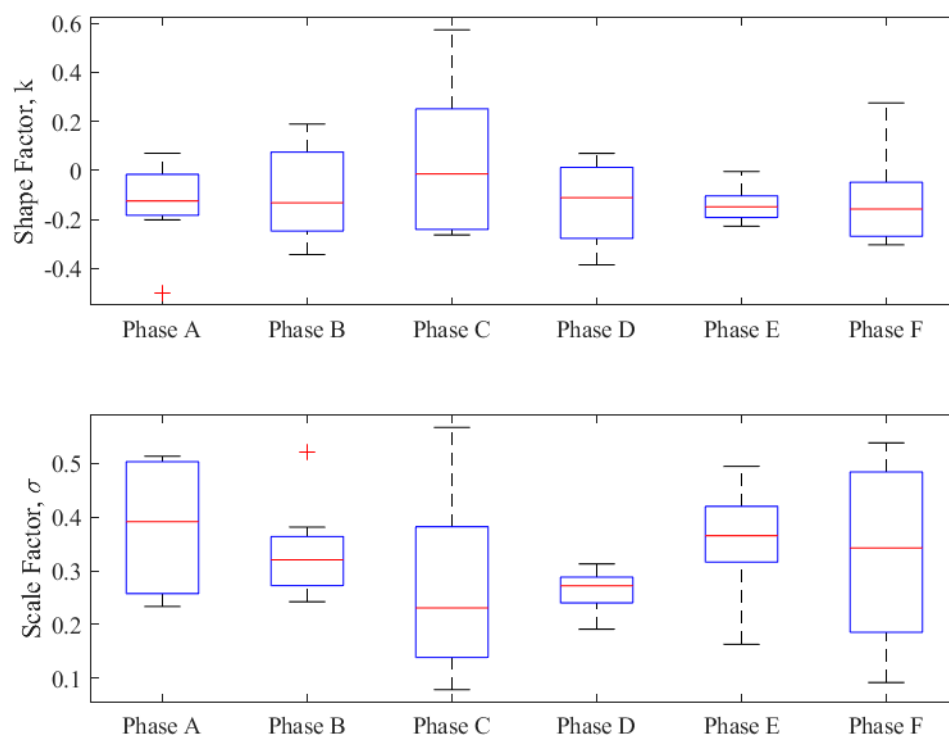


Figure 16. Generalised Pareto probability density function (PDF) fits to acceleration exceedance data from Bret 7 wave tests, for (a) Phase A; (b) Phase B; (c) Phase C; (d) Phase D; (e) Phase E and (f) Phase F.

Table 8. The generalised Pareto (GP) distribution parameter values for different phases of testing.

	<i>Bret</i> γ	Shape K	Scale Σ	Location μ
Phase A		0.072	0.563	1.054
Phase B		0.051	0.414	0.792
		−28.6%	−26.4%	−24.9%
Phase C		0.042	0.361	0.787
		−28.6%	−26.4%	−24.9%
Phase D		−0.017	0.341	0.689
		−123.9%	−39.4%	−34.6%
Phase E		0.022	0.554	1.091
		−69.3%	−1.6%	+3.6%
Phase F		0.146	0.548	1.010
		+103.3%	−2.6%	−4.2%

The changes to the shape of this distribution are described by the shape, scale and location factors and compared for the various testing phases. A change to the distribution of the maxima, as indicated by a change to the values of the shape and scale parameters, has the potential to be indicative of an overall change in state. The value of the location parameter did not vary, as the tails are all located above the p95 threshold and these were not investigated further. The boxplots in Figure 17 show the changes to both shape and scale factor values between phases. The values of each boxplot represent the values from all wave tests carried out at each phase. While a larger sample size will be able to quantify such changes accurately, the results indicate how a combination of the mean, interquartile range and tendency of outliers can link to the damage types exhibited in various test phases.

**Figure 17.** Boxplots showing the spread of scale and shape factors between all phases of testing.

5. Discussion and Conclusions

The results indicate how the various damage conditions reflect their impact on the dynamic responses of the floating platforms, but their characterisation requires extensive calibration.

Nevertheless, the changes and the extent of such changes may be better understood by looking into the distribution of the responses rather than isolated single point estimates. Scaling aspects and other uncertainties in models, especially in lower technological readiness levels, will continue to play a role in terms of uncertainty in the wave basin testing results, but extensive experimental characterisation and calibration similar to this paper have the potential to create robust markers of common damage or intervention events in the future. The natural frequencies of the platforms are low and thus change to their structural conditions due to damage, and other interventions can lead to a relatively significant change in such natural frequencies and cause increases or decreases in the peak responses to be more unreliable marker of such changes. In the future, extensive work is required under controlled levels of damage for different wave conditions so that a dependable and robust marker or a vector of markers can be created which can consistently reflect the extent of such damage. Such experiments can also provide better estimates of remaining capacity in terms of safety or serviceability performance. Research in the direction presented in this paper can thus lead to a significantly better understanding of lifetime safety of renewable energy device platforms at an early conceptual stage and lead to reduction in uncertainties around the structural behaviour of the system. Experimental investigation of damage state is an under-researched area and will be a much required topic in the future. Since efficient energy generation is related to lifetime structural safety and serviceability of such structures, it will eventually contribute to a more reliable and competitive generation of renewable energy. This paper contributed to this gap by investigating the possibilities and limitations of distinguishing various damage conditions in a spar buoy platform from its dynamic responses when exposed to Froude-scaled waves typical for the west coast of Ireland in an ocean wave basin. Scaled testing in an ocean wave basin is the most common method of increasing technological readiness levels of offshore renewable energy platforms, and the possibilities and limitations of such detection is thus particularly relevant for understanding their lifetime performance and safety. Five different structural modifications related to damage conditions were tested with respect to the undamaged condition in this paper for the spar platform and investigated for their acceleration responses. The work addresses the paucity in experimental literature investigating the uncertainty and reliability of such damage responses and their detection, which, in turn, can inform and provide a limit to what can be reasonably achieved from actual tests, where only the output responses are typically available in relative detail. The following observations were noted:

1. Free decay tests and estimates of natural frequency and damping ratios from such tests are not particularly useful to detect the presence of differentiation between the levels of types of damage.
2. Mean and p95 percentiles show changes when there is a significant variation in the structure, but they do not show a distinct pattern to distinguish types and extents of damage.
3. Best fit distributions on measured histograms of acceleration responses of the structure indicate significant changes in various damage phases, and the distribution parameters, once calibrated against the type of damage condition, can be helpful in determining the damage or an effect of a change that is equivalent to the calibrated damage condition.
4. Extreme value distribution fits to the tails of the measured histograms indicate that changes in distribution parameters can be calibrated against the damage conditions. A calibrated combination of the parameters of the distribution fits for the overall and the extremes from the measured histograms can thus be relevant for characterizing damages.

Author Contributions: Conceptualisation, V.P. and J.M.; methodology, D.O., J.M. and V.P.; software, D.O., J.M. and V.P.; validation, D.O., J.M. and V.P.; formal analysis, D.O.; investigation, D.O., J.M. and V.P.; resources, J.M. and V.P.; data curation, D.O.; writing—original draft preparation, D.O., V.P. and J.M.; writing—review and editing, V.P. and J.M.; visualisation, D.O.; supervision, V.P. and J.M.; project administration, V.P.; funding acquisition, V.P. All authors have read and agreed to the published version of the manuscript.

Funding: This research was funded by Science Foundation Ireland, Marine and Renewable Energy Ireland (MaREI) Centre and the Irish Research Council IRC GOIPG/2016/71.

Acknowledgments: V.P. and D.O. wish to acknowledge The Energy Institute, University College Dublin, Ireland.

Conflicts of Interest: The authors declare no conflict of interest.

References

1. Topham, E.; McMillan, D. Sustainable decommissioning of an offshore wind farm. *Renew. Energy* **2017**, *102*, 470–480. [CrossRef]
2. Martinez-Luengo, M.; Kolios, A.; Wang, L. Structural health monitoring of offshore wind turbines: A review through the Statistical Pattern Recognition Paradigm. *Renew. Sustain. Energy Rev.* **2016**, *64*, 91–105. [CrossRef]
3. National Research Council (US). Transportation Research Board Structural Integrity of Offshore Wind Turbines. In *Structural Integrity of Offshore Wind Turbines*; The National Academies Press: Washington, DC, USA, 2011; Volume 305. [CrossRef]
4. Etemaddar, M.; Blanke, M.; Gao, Z.; Moan, T. Response analysis and comparison of a spar-type floating offshore wind turbine and an onshore wind turbine under blade pitch controller faults. *Wind. Energy* **2014**, *19*, 35–50. [CrossRef]
5. Seo, B.; Shin, H.; Kim, J.; Shim, W.; Ahn, H.; Yu, Y.; Dam, P.T.; Kumar, R. A Study on Structural Responses of Offshore Wind Turbines by Slamming Loads. In Proceedings of the ASME 2018 1st International Offshore Wind Technical Conference, San Francisco, CA, USA, 4–7 November 2018.
6. Sun, C. Mitigation of offshore wind turbine responses under wind and wave loading: Considering soil effects and damage. *Struct. Control Health Monit.* **2017**, *25*, e2117. [CrossRef]
7. Wang, C.; Utsunomiya, T.; Wee, S.C.; Choo, Y.S. Research on floating wind turbines: A literature survey. *IES J. Part A Civ. Struct. Eng.* **2010**, *3*, 267–277. [CrossRef]
8. Watson, S.J.; Moro, A.; Reis, V.; Baniotopoulos, C.; Barth, S.; Bartoli, G.; Bauer, F.; Boelman, E.; Bosse, D.; Cherubini, A.; et al. Future emerging technologies in the wind power sector: A European perspective. *Renew. Sustain. Energy Rev.* **2019**, *113*, 109270. [CrossRef]
9. DNVGL-OS-C105. *Structural Design of TLPs—LRFD Method*. 2015. Available online: <https://rules.dnvgl.com/docs/pdf/dnvgl/os/2015-07/DNVGL-OS-C105.pdf> (accessed on 13 July 2020).
10. Ochi, M.K. *Ocean Waves: The Stochastic Approach (Volume 6)*; Cambridge University Press (Cambridge Ocean Technology Series): Cambridge, UK, 2005. [CrossRef]
11. O’Kelly-Lynch, P.; Long, C.; McAuliffe, F.D.; Murphy, J.; Pakrashi, V. Structural design implications of combining a point absorber with a wind turbine monopile for the east and west coast of Ireland. *Renew. Sustain. Energy Rev.* **2020**, *119*, 109583. [CrossRef]
12. Bachynski, E.E.; Moan, T. Design considerations for tension leg platform wind turbines. *Mar. Struct.* **2012**, *29*, 89–114. [CrossRef]
13. Barranco-Cicilia, F.; Lima, E.; Sagrilo, L. Reliability-based design criterion for TLP tendons. *Appl. Ocean Res.* **2008**, *30*, 54–61. [CrossRef]
14. Xu, K.; Zhang, M.; Shao, Y.; Gao, Z.; Moan, T. Effect of wave nonlinearity on fatigue damage and extreme responses of a semi-submersible floating wind turbine. *Appl. Ocean Res.* **2019**, *91*, 101879. [CrossRef]
15. Ma, Z.; Li, W.; Ren, N.; Ou, J. The typhoon effect on the aerodynamic performance of a floating offshore wind turbine. *J. Ocean Eng. Sci.* **2017**, *2*, 279–287. [CrossRef]
16. Ciang, C.C.; Lee, J.-R.; Bang, H.-J. Structural health monitoring for a wind turbine system: A review of damage detection methods. *Meas. Sci. Technol.* **2008**, *19*, 122001. [CrossRef]
17. Zhang, Z.; Li, J.; Zhuge, P. Failure Analysis of Large-Scale Wind Power Structure under Simulated Typhoon. *Math. Probl. Eng.* **2014**, *2014*, 1–10. [CrossRef]
18. Soman, R. Semi-automated methodology for damage assessment of a scaled wind turbine tripod using enhanced empirical mode decomposition and statistical analysis. *Int. J. Fatigue* **2020**, *134*, 105475. [CrossRef]
19. Siddiqui, M.; Greco, M.; Lugni, C.; Faltinsen, O. Experimental studies of a damaged ship section in beam sea waves. *Appl. Ocean Res.* **2020**, *97*, 102090. [CrossRef]
20. Draycott, S.; Steynor, J.; Nambiar, A.; Sellar, B.; Venugopal, V. Experimental assessment of tidal turbine loading from irregular waves over a tidal cycle. *J. Ocean Eng. Mar. Energy* **2019**, *5*, 173–187. [CrossRef]
21. Jaksic, V.; Wright, C.S.; Murphy, J.; Afeef, C.; Ali, S.F.; Mandic, D.P.; Pakrashi, V. Dynamic response mitigation of floating wind turbine platforms using tuned liquid column dampers. *Philos. Trans. R. Soc. A Math. Phys. Eng. Sci.* **2015**, *373*, 20140079. [CrossRef]

22. Jaksic, V.; O'Shea, R.; Cahill, P.; Murphy, J.; Mandic, D.P.; Pakrashi, V. Dynamic response signatures of a scaled model platform for floating wind turbines in an ocean wave basin. *Philos. Trans. R. Soc. A Math. Phys. Eng. Sci.* **2015**, *373*, 20140078. [[CrossRef](#)]
23. O'Donnell, D.; Srbnovsky, B.; Murphy, J.; Popovici, E.; Pakrashi, V. Sensor Measurement Strategies for Monitoring Offshore Wind and Wave Energy Devices. In Proceedings of the 11th International Conference on Damage Assessment of Structures (DAMAS 2015), Ghent, Belgium, 24–26 August 2015; Volume 628, p. 012117. [[CrossRef](#)]
24. Damiani, R.R. *Uncertainty and Risk Assessment in the Design Process for Wind*; National Renewable Energy Lab (NREL): Golden, CO, USA, 2018.
25. Leimeister, M.; Kolios, A. A review of reliability-based methods for risk analysis and their application in the offshore wind industry. *Renew. Sustain. Energy Rev.* **2018**, *91*, 1065–1076. [[CrossRef](#)]
26. Yeter, B.; Tekgoz, M.; Garbatov, Y.; Soares, C.G. Fragility analysis of an ageing monopile offshore wind turbine subjected to simultaneous wind and seismic load. *Saf. Extreme Environ.* **2020**, 1–16. [[CrossRef](#)]
27. Quilligan, A.; O'Connor, A.; Pakrashi, V. Fragility analysis of steel and concrete wind turbine towers. *Eng. Struct.* **2012**, *36*, 270–282. [[CrossRef](#)]
28. Pakrashi, V.; Fitzgerald, P.; O'Leary, M.; Jaksic, V.; Ryan, K.; Basu, B. Assessment of structural nonlinearities employing extremes of dynamic responses. *J. Vib. Control* **2016**, *24*, 137–152. [[CrossRef](#)]
29. Pakrashi, V.; O'Shea, R.; Jaksic, V.; Murphy, J. The Hurst Exponent as an Indicator of the Behaviour of a Model Monopile in an Ocean Wave Testing Basin. In Proceedings of the 11th International Conference on Damage Assessment of Structures (DAMAS 2015), Ghent, Belgium, 24–26 August 2015; Volume 628, p. 012057. [[CrossRef](#)]
30. Jaksic, V.; Mandic, D.P.; Ryan, K.; Basu, B.; Pakrashi, V. A comprehensive study of the delay vector variance method for quantification of nonlinearity in dynamical systems. *R. Soc. Open Sci.* **2016**, *3*, 150493. [[CrossRef](#)] [[PubMed](#)]
31. O'Leary, K.; Pakrashi, V.; Kelliher, D. Optimization of composite material tower for offshore wind turbine structures. *Renew. Energy* **2019**, *140*, 928–942. [[CrossRef](#)]
32. Wright, C.; Pakrashi, V.; Murphy, J. Dynamic Effects of Anchor Positional Tolerance on Tension Moored Floating Wind Turbine. *J. Phys. Conf. Ser.* **2016**, *753*, 92019. [[CrossRef](#)]
33. Wright, C.; O'Sullivan, K.; Murphy, J.; Pakrashi, V. Experimental Comparison of Dynamic Responses of a Tension Moored Floating Wind Turbine Platform with and without Spring Dampers. In Proceedings of the 11th International Conference on Damage Assessment of Structures (DAMAS 2015), Ghent, Belgium, 24–26 August 2015; Volume 628, p. 012056. [[CrossRef](#)]
34. Chortis, G.; Askarinejad, A.; Prendergast, L.J.; Li, Q.; Gavin, K. Influence of scour depth and type on p–y curves for monopiles in sand under monotonic lateral loading in a geotechnical centrifuge. *Ocean Eng.* **2020**, *197*, 106838. [[CrossRef](#)]
35. Prendergast, L.J.; Reale, C.; Gavin, K. Probabilistic examination of the change in eigenfrequencies of an offshore wind turbine under progressive scour incorporating soil spatial variability. *Mar. Struct.* **2018**, *57*, 87–104. [[CrossRef](#)]
36. Jamalkia, A.; Ettetfagh, M.M.; Mojtahedi, A. Damage detection of TLP and Spar floating wind turbine using dynamic response of the structure. *Ocean Eng.* **2016**, *125*, 191–202. [[CrossRef](#)]
37. Chen, J.; Hu, Z.; Duan, F. Comparisons of dynamical characteristics of a 5 MW floating wind turbine supported by a spar-buoy and a semi-submersible using model testing methods. *J. Renew. Sustain. Energy* **2018**, *10*, 053311. [[CrossRef](#)]
38. Cruz, J.; Acheson, M. (Eds.) *Floating Offshore Wind Energy: The Next Generation of Wind Energy*; Springer: Cham, Switzerland, 2016.
39. Roddier, D.; Cermelli, C.; Aubault, A.; Weinstein, A. Wind Float: A floating foundation for offshore wind turbines. *J. Renew. Sustain. Energy* **2010**, *2*, 033104. [[CrossRef](#)]
40. Moan, T. Integrity Management of Offshore Structures With Emphasis on Design for Structural Damage Tolerance. *J. Offshore Mech. Arct. Eng.* **2020**, *142*, 1–65. [[CrossRef](#)]
41. Wang, X.; Moan, T. Stochastic and deterministic combinations of still water and wave bending moments in ships. *Mar. Struct.* **1996**, *9*, 787–810. [[CrossRef](#)]
42. Chiang, A.C.; Keoleian, G.A.; Moore, M.R.; Kelly, J.C. Investment cost and view damage cost of siting an offshore wind farm: A spatial analysis of Lake Michigan. *Renew. Energy* **2016**, *96*, 966–976. [[CrossRef](#)]

43. Shanley, M. Innovative Hull Design for Servicing Offshore Wind Turbines. Ph.D. Thesis, University College Cork, Cork, Ireland, 2018.
44. Desmond, C.; Buret, B.; Shanley, M.; Murphy, J.; Pakrashi, V. The Assessment of Water Surface Elevation Uncertainty in a Hydraulics Laboratory. In Proceedings of the 13th International Conference on Applications of Statistics and Probability in Civil Engineering (ICASP13), Seoul, Korea, 26–30 May 2019.
45. Chakrabarti, S. Physical model testing of floating offshore structures. In Proceedings of the Dynamic Positioning Conference, Houston, TX, USA, 13–14 October 1998; Volume 1, pp. 1–33.
46. Larsen, T.; Hanson, T.D. A method to avoid negative damped low frequent tower vibrations for a floating, pitch controlled wind turbine. In Proceedings of the Science of Making Torque from Wind, Copenhagen, Denmark, 28–31 August 2007; Volume 75, p. 12073. [[CrossRef](#)]
47. Sethuraman, L.; Xing, Y.; Gao, Z.; Venugopal, V.; Mueller, M.; Moan, T. A 5MW direct-drive generator for floating spar-buoy wind turbine: Development and analysis of a fully coupled Mechanical model. *Proc. Inst. Mech. Eng. Part A J. Power Energy* **2014**, *228*, 718–741. [[CrossRef](#)]
48. Tucker, M.J.; Pitt, E.G. *Waves in Ocean Engineering (No. Volume 5)*; Elsevier Science & Technology: Oxford, UK, 2001.
49. Cahill, B. Characteristics of the Wave Energy Resource at the Atlantic Marine Energy Test Site. Ph.D. Thesis, University College Cork, Cork, Ireland, 2013.
50. Yang, H.; Xu, P. Effect of hull geometry on parametric resonances of spar in irregular waves. *Ocean Eng.* **2015**, *99*, 14–22. [[CrossRef](#)]
51. Gavassoni, E.; Gonçalves, P.B.; Roehl, D.M. Nonlinear vibration modes and instability of a conceptual model of a spar platform. *Nonlinear Dyn.* **2013**, *76*, 809–826. [[CrossRef](#)]
52. Jingrui, Z.; Yougang, T.; Wenjun, S. A Study on the Combination Resonance Response of a Classic Spar Platform. *J. Vib. Control* **2010**, *16*, 2083–2107. [[CrossRef](#)]
53. Ay, A.M.; Khoo, S.; Wang, Y. Probability distribution of decay rate: A statistical time-domain damping parameter for structural damage identification. *Struct. Health Monit.* **2018**, *18*, 66–86. [[CrossRef](#)]
54. Carden, E.P.; Fanning, P. Vibration Based Condition Monitoring: A Review. *Struct. Health Monit.* **2004**, *3*, 355–377. [[CrossRef](#)]
55. Carden, E.P.; Brownjohn, J.M. ARMA modelled time-series classification for structural health monitoring of civil infrastructure. *Mech. Syst. Signal Process.* **2008**, *22*, 295–314. [[CrossRef](#)]
56. Kullaa, J. Damage detection of the z24 bridge using control charts. *Mech. Syst. Signal Process.* **2003**, *17*, 163–170. [[CrossRef](#)]
57. Bali, S.; Hazra, B.; Pakrashi, V. Quantile autoregressive modeling for non-linear change detection in vibrating structural systems. *Mech. Res. Commun.* **2019**, *100*, 103397. [[CrossRef](#)]
58. Joseph, G.V.; Hao, G.; Pakrashi, V. Fragility analysis using vibration energy harvesters. *Eur. Phys. J. Spec. Top.* **2019**, *228*, 1625–1633. [[CrossRef](#)]
59. Joseph, G.V.; Hao, G.; Pakrashi, V. Extreme value estimates using vibration energy harvesting. *J. Sound Vib.* **2018**, *437*, 29–39. [[CrossRef](#)]
60. Rocher, B.; Schoefs, F.; François, M.; Salou, A.; Caouiissin, A.-L. A two-scale probabilistic time-dependent fatigue model for offshore steel wind turbines. *Int. J. Fatigue* **2020**, *136*, 105620. [[CrossRef](#)]
61. Radhika, B.; Manohar, C. Reliability models for existing structures based on dynamic state estimation and data based asymptotic extreme value analysis. *Probabilistic Eng. Mech.* **2010**, *25*, 393–405. [[CrossRef](#)]
62. Begovic, E.; Bertorello, C.; Pennino, S.; Piscopo, V.; Scamardella, A. Statistical analysis of planing hull motions and accelerations in irregular head sea. *Ocean Eng.* **2016**, *112*, 253–264. [[CrossRef](#)]
63. Dong, W.; Moan, T.; Gao, Z. Fatigue reliability analysis of the jacket support structure for offshore wind turbine considering the effect of corrosion and inspection. *Reliab. Eng. Syst. Saf.* **2012**, *106*, 11–27. [[CrossRef](#)]
64. Soares, C.G.; Carvalho, A. Probability distributions of wave heights and periods in combined sea-states measured off the Spanish coast. *Ocean Eng.* **2012**, *52*, 13–21. [[CrossRef](#)]

